scientific reports

Check for updates

OPEN

Developmental changes in brain structure and function following exposure to oral LSD during adolescence

Lila Harris-Blum[1], Zachary Smith[1], Richard J. Ortiz[2], Deepti Athreya[1], Arnold Chang[1], Praveen P. Kulkarni[1] & Craig F. Ferris[1,3]✉

LSD is a hallucinogen with complex neurobiological and behavioral effects. Underlying these effects are changes in brain neuroplasticity. This is the first study to follow the developmental changes in brain structure and function following LSD exposure in periadolescence. We hypothesized LSD given during a time of heightened neuroplasticity, particularly in the forebrain, would affect cognitive and emotional behavior and the associated underlying neuroanatomy and neurocircuitry. Female and male mice were given vehicle, single or multiple treatments of 3.3 µg of LSD by oral gavage starting on postnatal day 51. Between postnatal days 90–120 mice were imaged and tested for cognitive and motor behavior. MRI data from voxel-based morphometry, diffusion weighted imaging, and BOLD resting state functional connectivity were registered to a mouse 3D MRI atlas with 139 brain regions providing site-specific differences in global brain structure and functional connectivity between experimental groups. Motor behavior and cognitive performance were unaffected by periadolescent exposure to LSD. Differences across experimental groups in brain volume for any of the 139 brain areas were few in number and not focused on any specific brain region. Multiple exposures to LSD significantly altered gray matter microarchitecture across much of the brain. These changes were primary associated with the thalamus, sensory and motor cortices, and basal ganglia. The forebrain olfactory system and prefrontal cortex and hindbrain cerebellum and brainstem were unaffected. The functional connectivity between forebrain white matter tracts and sensorimotor cortices and hippocampus was reduced with multidose LSD exposure. Does exposure to LSD in late adolescence have lasting effects on brain development? The bulk of our significant findings were seen through changes is DWI values across 74 brain areas in the multi-dose LSD group. The pronounced changes in indices of anisotropy across much of the brain would suggest altered gray matter microarchitecture and neuroplasticity. There was no evidence of LSD having consequential effects on cognitive or motor behavior when animal were evaluated as young adults 90–120 days of age. Neither were there any differences in the volume of specific brain areas between experimental conditions. The reduction in connectivity in forebrain white matter tracts with multidose LSD and consolidation around sensorimotor and hippocampal brain areas requires a battery of tests to understand the consequences of these changes on behavior.

Keywords Diffusion weighted imaging, Voxel based morphometry, Neuroplasticity, Resting state functional connectivity, Sensorimotor cortex

Lysergic Acid Diethylamide (LSD) is a psychoactive compound first synthesized in the mid-twentieth century[1]. Early research with LSD focused primarily on its behavioral and therapeutic effects. The original findings showed promising potential for using LSD in treating various mental disorders such as major depressive disorder (MDD), post-traumatic stress disorder (PTSD), and addiction[2]. Amidst the War on Drugs in 1971, the United Nations classified LSD and other psychedelic drugs as Schedule 1 substances, and research halted[2]. However, in the past

[1]Center for Translational NeuroImaging, Northeastern University, Boston, MA, USA. [2]Department of Chemistry and Biochemistry, New Mexico State University, Las Cruces, NM, USA. [3]Department of Psychology and Pharmaceutical Sciences, Northeastern University, 125 NI Hall, 360 Huntington Ave, Boston, MA 02115-5000, USA. ✉email: c.ferris@northeastern.edu

decade, there has been a resurgence of scientific interest in LSD. Small clinical trials report promising results in treating MDD, end-of-life distress, PTSD, and alcoholism[2,3]. The ways that LSD affects neural circuitry to alter behavior are not well known.

Functional MRI is a non-invasive method for characterizing changes in brain function and connectivity in response to CNS therapeutics[4–7] There have been several functional imaging studies on healthy volunteers attempting to map specific pathways attributable to the psychedelic experience of LSD[8–10]. They are all very similar in design. A single dose of LSD is given orally or IV outside the scanner. Sixty to 150 min later, subjects are imaged for changes in resting-state functional connectivity (rsFC) as compared to data collected following placebo. In general, they report similar changes in brain activity across several major brain areas. There is an increase in thalamo-cortical connectivity that may account for visual hallucinations, and a decrease in activity in the parahippocampus that may contribute to the dysregulation of the resting-state and 'maintenance of the self' or 'consciousness' as we currently understand[8,11]. Further research has shown the mechanisms of LSD involves the 5-HT2a receptor. When LSD is administered with a 5-HT2a antagonist, the subjective effects of LSD are diminished[12,13].

Patients with various psychiatric conditions, e.g., MDD, anxiety, substance abuse disorder, when treated with the classical hallucinogenic 5HT2a receptor agonists, show improvement that may last for months[14–17]. These sustained positive effects are evidence of neuroplastic changes in brain neural circuitry[18]. Indeed, there are several reports of increased dendritic arborization and dendritic spines density following treatment with hallucinogens, particularly LSD[19], The mechanism target of rapamycin (mTOR), a protein kinase, has a key role in regulating neuronal growth and proliferation contributing to the enhanced neuroplasticity with hallucinogens[19]. Preclinical studies following the long-term effects of LSD routinely look for changes in locomotor function and anxiety. For example, after chronic exposure to LSD, mice exhibited spontaneous hyperactivity in the absence of a challenge dose[20]. Interestingly, to the best of our knowledge, there have been no preclinical or clinical studies on the long-term developmental consequences of LSD use in periadolescence.

Adolescence, in neuroscience, is defined as the developmental period beginning with the onset of puberty and ending with the pruning of neural pathways to the prefrontal cortex (PFC)[21]. The start of puberty is highlighted by the activity of androgens in neural pathways, and the end is distinguished by the solidification of inhibitory function of the PFC on lower brain areas[22], which generally occurs at age 25–28 in humans[23]. LSD use in adolescence age 12–17 and 18–25 has increased in the past decade[24]. In 2019, 4% of the 18–25 age group reported LSD use in the past 12 months[24]. The long-term effects of LSD on the developing adolescent brain are not known. The prevalence and trends of LSD use in adolescents warrants research on the drug's effects in later life. The present study examines male and female mice exposed to LSD during periadolescence. Animals were studied in early adulthood 90–120 days of age, for changes in neurobiology using multimodal MRI and behavioral assays testing for motor control and cognitive function. To enhance the translational aspect of our findings, the first dose of LSD was administered at age P51, which, in mice (P50-P60), is neurodevelopmentally equivalent to late adolescence in humans[25].

Methods

Animals

Thirty-six C57BL/J6 mice, half male/half female, forty-five days of age were obtained from Charles River Laboratories (Wilmington, Massachusetts, USA). Animals were housed in plastic cages (3–5 per cage) and maintained in ambient temperature (22–24 °C) on a 12:12 reverse light:dark cycle (lights off at 09:00 h). All experiments were started on postnatal day 51 and conducted under dim red illumination between 10:00 h and 18:00 h to avoid the transitions between the L–D dark cycle. Food and water were provided ad libitum. All animals were acquired and cared for in accordance with the guidelines published in the NIH Guide for the Care and Use of Laboratory Animals. All methods and procedures described below were pre-approved by the Northeastern University Institutional Animal Care and Use Committee under protocol number 23-0407R. Northeastern University's animal care and use program and housing facilities are fully accredited by AAALAC, International.The protocols used in this study followed the ARRIVE guidelines for reporting in vivo experiments in animal research[26].

LSD preparation and administration

LSD was acquired from the National Institute on Drug Abuse (NIH/NIDA, Bethesda, MD) through the Research Triangle Institute (Research Triangle Park, NC). Animals were randomly divided into three groups: vehicle, single-dose LSD, and multi-dose LSD. Body weights ranged between 20 and 24 g. Each mouse received a 100 µl gavage (syringe 2″-curved needle w/2 mm ball-tip) for an approximate dose of 3.3 µg of LSD or 70 µg/kg. The dose was chosen based on low-moderate doses used in other pre-clinical studies[27–30]. Head twitching was observed within minutes of treatment. The vehicle group received a comparable volume 0.9% saline. The multi-dose group was gavaged a total of six times over 14 days. Time between treatments varied between 2 and 3 days. One mouse from the multi-dose group died for reasons unknown.

Image set-up and data acquisition

A detailed description of the mouse imaging system is published elsewhere[31]. Notably, we used a quadrature transmit/receive volume coil (ID = 38 mm) that provided both high anatomical resolution and high signal-to-noise ratio for voxel-based BOLD fMRI (Ekam Imaging, Boston, MA, USA). The design of the coil provided complete coverage of the brain from olfactory bulbs to brain stem with excellent B1 field homogeneity. The design of the restraining system included a padded head support obviating the need for ear bars helping to reduce animal discomfort while minimizing motion artifact. All mice were imaged while under light 1% isoflurane anesthesia for a maximum of 1 h as previously described[32]. The respiration rate were between 50 and 55 breaths/min.

Imaging sessions were conducted under dim-red illumination using a Bruker Biospec 7.0 T/20-cm USR horizontal magnet (Bruker; Billerica, MA) and a 2 T/m magnetic field gradient insert (ID = 12 cm) capable of a 120-µsec rise time. At the beginning of each imaging session, a high-resolution anatomical data set was collected using the rapid acquisition relaxation enhancement (RARE) pulse sequence (RARE factor 8); (18 slices; 0.75 mm; field of view (FOV) 1.8 cm^2; data matrix 128 × 128; repetition time (TR) 2.1 s; echo time (TE) 12.4 ms; Effect TE 48 ms; number of excitations (NEX) 6; 6.5 min acquisition time). All mice were imaged between six to eight weeks following their first exposure to LSD.

Voxel based morphometry

A 3D Mouse Brain Atlas© with 139 segmented and annotated brain regions (Ekam Solutions; Boston, MA) was used to calculate brain volumes, and register the standard structural mouse template image onto the high resolution T2-weighted images for each individual subject using a non-linear registration method implemented by Unix based software package Deformable Registration via Attribute Matching and Mutual-Saliency Weighting (DRAMMS; https://www.cbica.upenn.edu/sbia/software/dramms/index.html). The atlas (image size 256 × 256 × 63) was then warped from the standard space into the subject image space (image size 256 × 256 × 40) using the deformation obtained from the previous step and the nearest-neighbor interpolation method. In the volumetric analysis, each brain region was therefore segmented, and the volume values extracted for all 139 ROIs, calculated by multiplying unit volume of voxel in mm^3 by the number of voxels using an in-house MATLAB script (available upon request). To account for different brain sizes all the ROI volumes were normalized by dividing each ROI volume by total brain volume of that subject.

Differences in brain volumes (mm^3) between 139 areas were compared across each of the three experimental conditions using a Kruskal-Wallace nonparametric multiple comparisons test. The percentage difference in volume between brain areas was calculated to normalize the data and correct for large differences in brain volumes between areas (e.g., caudate/putamen 16 mm^3; accumbens core 1.4 mm^3).

Diffusion weighted imaging—quantitative anisotropy

Diffusion weighted imaging (DWI) was acquired with a spin-echo echo-planar-imaging (EPI) pulse sequence as previously described[33–35] having the following parameters: TR/TE = 500/20 ms, eight EPI segments, and ten non-collinear gradient directions with a single b-value shell at 1000 s/mm^2 and one image with a B-value of 0 s/mm^2 (referred to as B0). Geometrical parameters were: 25 coronal slices, each 0.281 mm thick (brain volume) and with in-plane resolution of 0.281 × 0.281 mm^2 (matrix size 64 × 64; FOV 18 mm^2) with a 36 min acquisition time. Image reconstruction included DWI analysis of the DW-3D-EPI images to produce the maps of fractional anisotropy (FA) and apparent diffusion coefficient (ADC). DWI analysis was implemented with MATLAB and MedINRIA (1.9.0; http://www.sop.inria.fr/asclepios/software/MedINRIA/index.php) software. Because sporadic excessive breathing during DWI acquisition can lead to significant image motion artifacts that are apparent only in the slices sampled when motion occurred, each image (for each slice and each gradient direction) was screened, prior to DWI analysis, for motion artifacts; if found, acquisition points with motion artifacts were eliminated from the analysis.

For statistical comparisons between mice, each brain volume was registered to the mouse atlas allowing voxel- and region-based statistics. All image transformations and statistical analyses were conducted using the in-house MIVA software. For each vole, the B0 image was co-registered with the B0 template (using a 6-parameter rigid-body transformation). The co-registration parameters were then applied to the DWI indexed maps for the different indices of anisotropy. Normalization was performed on the maps since they provided the most detailed and accurate visualization of brain structures and allowed for more accurate normalization. Normalization parameters were then applied to all DWI indexed maps. Normalized indexed maps were smoothed with a 0.3-mm Gaussian kernel. To ensure that the anisotropy values were not affected significantly by the pre-processing steps, the 'nearest neighbor' option was used following registration and normalization. Statistical differences in measures of DWI between experimental groups were determined using a nonparametric Mann–Whitney U Test (alpha set at 5%). The formula below was used to account for false discoveries from multiple comparisons.

$$P(i) \leq \frac{i}{V}\frac{q}{c(V)}$$

P(i) is the p-value based on the t-test analysis. Each of 139 ROIs (i) within the brain containing (V) ROIs was ranked in order of its probability value. The false-positive filter value q was set to 0.2 and the predetermined c(V) set at unity.

Resting state functional connectivity

Preprocessing in this study was accomplished by combining Analysis of Functional NeuroImages (AFNI_17.1.12, http://afni.nimh.nih.gov/afni/), FMRIB Software library (FSL, v5.0.9, http://fsl.fmrib.ox.ac.uk/fsl/), Deformable Registration via Attribute Matching and Mutual-Saliency Weighting (DRAMMS 1.4.1, https://www.cbica.upenn.edu/sbia/software/dramms/index.html), and MATLAB (Mathworks, Natick, MA, USA) as previously described[35,36]. Brain tissue masks for resting-state functional images were manually drawn using 3DSlicer (https://www.slicer.org/) and applied for skull stripping. Motion outliers (i.e., data corrupted by extensive motion) were detected in the dataset and the corresponding time points were recorded and regressed out in a later step. Functional data were assessed for the presence of motion spikes. Any large motion spikes were identified and removed from the time-course signals. This filtering step was followed by slice timing correction from interleaved slice acquisition order. Head motion corrections (six motion parameters) were conducted using the first volume as

a reference image. Normalization was completed by registering functional data to the mouse atlas using affine registration through DRAMMS. After quality assurance, band-pass filtering (0.01–0.1 Hz) was performed to reduce low-frequency drift effects and high-frequency physiological noise for each subject. The resulting images were further detrended and spatially smoothed (full width at half maximum = 0.8 mm). Finally, regressors comprised of motion outliers, the six motion parameters, the mean white matter, and cerebrospinal fluid time series were fed into general linear models for nuisance regression to remove unwanted effects. The region-to-region functional connectivity method was performed in this study to measure the correlations in spontaneous BOLD fluctuations. Briefly, a network is comprised of nodes and edges; nodes being the brain region of interest (ROI) and edges being the connections between regions. 139 nodes were defined using the ROIs segmented from the mouse atlas. Voxel time series data were averaged in each node based on the residual images using the nuisance regression procedure. Pearson's correlation coefficients across all pairs of nodes were computed for each subject among all three groups. The R-values (ranging from −1 to 1) are z-transformed using the Fisher's Z transform to improve normality. 139 × 139 symmetric connectivity matrices were constructed with each entry representing the strength of the edge. Group-level analysis was performed to look at the functional connectivity in all three experimental groups. The resulting Z-score matrices from one-group t-tests were clustered using the K-nearest neighbors clustering method to identify how nodes cluster together and form resting state networks. A Z-score threshold of $|Z| = 2.3$ was applied to remove spurious or weak node connections. The reasoning for 2.3 t-stat threshold is that it roughly corresponds to a 0.05 p-value (two-tailed). Voxel-wise seed analysis was also applied to study the temporal correlation of seed regions to the whole brain. The average time-course of BOLD signals in the three seeds were acquired and used to obtain the parametric maps of Fisher's Z transformed correlation coefficients for each voxel for each subject. These maps were used to assess connectivity differences in the different experimental groups.

Resting state functional connectivity scans were collected using a spin-echo triple-shot EPI sequence (imaging parameters: matrix size = 64 × 64 × 18 (H × W × D), TR/TE = 1000/15 ms, voxel size = 0.281 × 0.281 × 0.8 mm, slice thickness = 0.8 mm, with 300 NR, time of acquisition 15 min. There are numerous studies detailing the benefits of multi-shot EPI in BOLD imaging[37–40]. We avoided using single shot EPI because of its severe geometrical distortion at high field strengths (≥ 7 T) and loss of effective spatial resolution as the readout period increases[38]. There is also the possibility of signal loss in single shot EPI due to accumulated magnetic susceptibility or field inhomogeneity[39].

Resting state BOLD functional connectivity analysis

Degree centrality

All network analysis was computed with Gephi, an open-source network analysis and visualization software[41]. Absolute values of the symmetric connectivity matrices were imported for each experimental condition, and edges were loaded as undirected networks.

Degree centrality analysis quantifies the number of connections a specific node has to the overall network. Degree centrality is defined as:

$$C_D(j) = \sum_{j=1}^{n} A_{ij}$$

where n is the number of rows in the matrix in the adjacency matrix A and the elements of the matrix are given by A_{ij}, the number of edges between nodes i and j.

Statistics

All statistical analysis for the graph theory analysis was performed using GraphPad Prism version 9.0.0 for macOS, GraphPad Software, San Diego, California USA, https://www.graphpad.com. Normality tests between group subregions were performed to determine if parametric or non-parametric assumptions were needed. Shapiro–Wilk's tests were performed to analyze normality assumption. Subregion degree centrality p-values that were greater than 0.05 were assumed to be normal. After assumptions of normality were validated, paired t-tests were used to compare degree centrality of the LSD and vehicle groups in various subregions. When necessary, a non-parametric Wilcoxon signed rank (WSR) test is performed if there is evidence against the normality assumption.

Open-field test

Open Field testing was used to assess anxiety, exploratory behaviors, and locomotor ability as previously described[35]. It is based on the natural tendency of an animal to explore and protect itself using avoidance which translates to a normal animal spending more time in the periphery of the open field along the walls of the arena than in the center (the most anxiogenic area). Three weeks after LSD administration, animals were placed in the periphery of the OF arena (1764 cm^2 Plexiglas box) and allowed to explore freely for 4 min. The testing arena was dimly illuminated with two 40 W incandescent red-light bulbs. The box was cleaned with 70% isopropyl alcohol between each test. The arena was segmented into 16 equivalent square zones (4 center, 12 periphery). All sessions were video recorded then uploaded ANY-Maze software for analysis. Two main variables were used to measure the long-term anxiolytic effects of LSD: time spent in center, and number of times center was entered. We also collected data on locomotion during the trials. Each measure for the three experimental groups was compared with a one-way ANOVA using GraphPad Prism.

Novel object preference (NOP) test

NOP was conducted four weeks after LSD exposure to assess the longitudinal cognitive effects of LSD use during adolescence. NOP consisted of one acclimation day (habituation), one day of familiarization, and a third day of testing for novel object recognition. The box and objects were cleaned with 70% isopropyl alcohol between each mouse exposure to eliminate olfactory cues.

At the start of the study, each mouse was placed in an empty 1764 cm^2 Plexiglas box for 3 min each for habituation. There were two phases that each mouse had to go through after habituation: the Familiar Phase and the Novel Phase. 24 h after habituation, the mice were placed in the same box with two identical objects for 5 min for familiarization. Two objects (toy pig and blue shape) with different size, color, and texture were used for the NOP test. Half of each testing group was familiarized with an identical set of either the blue toy or the toy pig. 18 h later, for the Novel Phase, the mice spent another 5 min in the box with one familiar object and one novel object. The Novel Phase was filmed and uploaded to ANY-Maze software for tracking and analysis. Recorded measures included total time spent investigating the novel object, total time investigating familiar object, number of investigations of each object, and discrimination between objects.

Investigation ratios (IR = time spent investigating the novel object/ time spent investigating both objects) were assessed using single-sample, two-tailed t-tests, and performance was compared to chance (i.e., IR = 0.5). An investigation ratio significantly greater than 0.5 indicates that the mice were spending more time with the novel object. Conversely, a ratio significantly smaller than chance was used as an index of a preference for the familiar object. Analysis was performed with GraphPad Prism.

Results

Open-field test and novel object recognition test

Shown in Fig. 1a are scatter plots (mean ± SD) of the time spent in the center of the open field arena and the overall distance traveled during the 4 min observation period for each experimental condition. The single-dose group was found to spend the most time in the center zone (27.98 s) and the multi-dose group had the lowest time in center zone (14.29 s). A one-way ANOVA showed a significant difference between conditions [$F_{(2,32)} = 3.00$, $p = 0.030$]. A Tukey's multiple comparison's post hoc test showed both the vehicle and multiple dose LSD conditions were significantly less than the single dose condition ($p < 0.05$). There were no significant differences between experimental groups for distance traveled ($F_{(2,32)} = 2.079$, $p = 0.141$). Figure 1b are scatter plots of the investigation ratio or time spent with the novel object as compared to both objects. A one-sample t test showed all experimental conditions were significantly greater than chance ($p < 0.0001$). While there were no differences between groups in investigation ratio there were subtle but significant differences in behavior toward the novel and familiar objects. The latency from the time the mice were introduced to the testing box and their approach to the novel object was significantly different between groups ($F_{(2, 31)} = 4.914$, $p = 0.014$). A post hoc test showed the multidose group was significantly less than vehicle ($p < 0.05$). The duration of time or a single bout mice spent with the familiar object was significantly different between groups ($F_{(2,32)} = 5.585$, $p = 0.008$). Tukey's post hoc test showed the multidose group was significantly greater than either vehicle or single dose groups ($p < 0.05$).

Voxel based morphometry

Shown in tables in Supplementary Excel File S1 are the significant changes in brain volumes (mm^3) between single and multidose LSD treatments as compared to vehicle. In both treatments the changes were minimal.

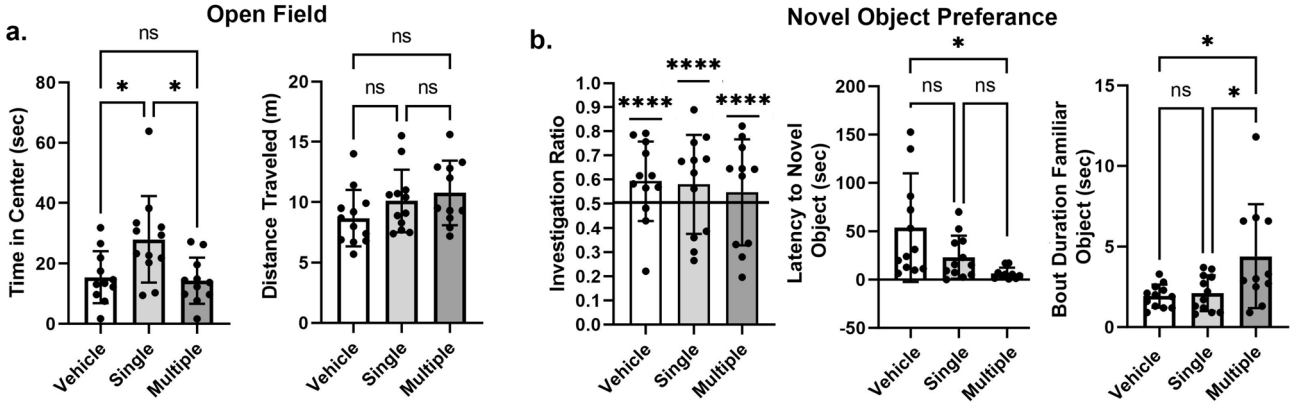

Figure 1. Behavior. Open field. (**a**) The scatter plots show the time spent in the center of the open field and the distanced traveled for each of the experimental conditions. Shown are the mean ± SD. The single dose LSD was significantly greater than vehicle or multiple dose for time spent in the center (*$p < 0.05$). Novel object preference. (**b**) Shown are scatter plots of the investigation ratio (time spent investigating the novel object/time spent investigating both objects). Performance was compared to chance (i.e., IR = 0.5) using single-sample, two-tailed t-tests. All experimental conditions were better than chance (****$p < 0.0001$). The latency to explore the novel object immediately after introduction to the chamber was significantly less for the multiple treatments as compared to vehicle and single treatment (*$p < 0.05$) The bout duration or time spent with the familiar objects at one exploration encounter was significantly greater for multiple treatments as compared to the other conditions (*$p < 0.05$). Shown are the mean ± SD.

Only 6/139 brain areas for either treatment showed significant change using a critical value of $p < 0.05$. A false discovery rate (FDR) for multiple comparison gave a significant level of $p = 0.008$.

Diffusion weighted imaging: apparent diffusion coefficient

Table 1 shows the significant changes in measures of ADC between vehicle and single dose LSD. Only 9/139 brain areas showed a significant difference. These areas are ranked in order of their significance. Reported is the mean and standard deviation (SD) for vehicle and LSD conditions together with probability values and the omega square (ω Sq) for effect size. The critical value was set at $p < 0.05$. An FDR for multi-comparisons gave a significant level of $p = 0.012$. In contrast, Table 2 lists 74/139 brains areas that showed significant changes following multiple dose LSD. In all cases, there was a greater measure of ADC with LSD treatment. The location of many of these brains areas are shown in the 2D maps and summarized in the 3D reconstructions in Fig. 2.

Shown in Table 3 are the significant changes in measures of FA between vehicle and single dose LSD. Only 11/139 brain areas showed a significant difference. An FDR for multi-comparisons gave a significant level of $p = 0.016$. Table 4 lists values for FA for multiple dose LSD. 17/139 brain areas showed a significant decrease in FA values. An FDR gave a significant value of $p = 0.024$. It is noteworthy that several areas associated with the ascending reticular activating system were affected e.g., pedunculopontine tegmentum, parabrachial n., locus coeruleus, pontine reticular n. and reticulotegmental n. Tables of FA and ADC values for all brain areas are found in Supplementary Excel Files S2 and S3, respectively.

Figure 2 shows the anatomical localization of the brain areas listed in Table 2 presented as statistical 2D heat maps. The coronal sections are labeled (a) through (i) and arranged from rostral (top) to caudal (bottom). Areas in blue were unaffected by the multidose LSD treatment while those in red were significantly increased in measures of ADC. Given the substantial number of affected areas, the locations are better summarized as brain regions. Note the conspicuous absence of any changes in the olfactory bulb (a) and prefrontal ctx (b) The basal ganglia (c, d), hypothalamus (d), sensory motor cortex (e), thalamus (f) midbrain (f, g) and cerebellum (h, i) are all significantly affected by adolescent exposure to multiple doses of LSD. Note the brainstem and pons (g–i) are unaffected.

Resting state functional connectivity

The percentage change in degrees (connections) for all 139 brain areas between multidose LSD and vehicle controls are shown in Fig. 3a as violin plots i.e., the probability distribution of the numerical data for each group and their mean difference (MD). The multidose group had significantly fewer connections (two-tailed, paired t-test, $p < 0.0001$). The vehicle global network density was 0.070 and the average degree 9.518. The multiple LSD global network density was 0.063 and the average degree 8.555.

When the brain areas were organized into 12 brain regions e.g., basal ganglia, olfactory system, hypothalamus, thalamus, cerebellum etc. (Supplementary Data Fig S1), there were no significant differences in degrees between vehicle and multidose groups with the exception of the somatosensory cortex. The bar graphs in Fig. 3b depict this significant difference (mean ± SD) between vehicle and multidose groups for the somatosensory ctx ($p < 0.01$).

Figure 4 depicts the degrees (connecting lines) and nodes (circles) arranged in a radial array between the forebrain white matter tracts comprised of the corpus callosum, forceps minor and external capsule collapsed as one single yellow node, cerebral nuclei (green), brainstem/cerebellar areas (red) hippocampal complex (pink) and basal ganglia (blue) for vehicle and multidose LSD treatments. The caudate/putamen is a major part of the basal ganglia. Nodes highlighted in black, e.g. claustrum, lateral septum, superior colliculus, do not represent a major part of any particular brain region. The superior colliculus in found in the midbrain and is involved in visual orientation. The septum is part of the forebrain involved in social behavior and emotion. The claustrum is a thin layer of cells beneath the somatosensory cortex thought to be involved in organizing communication between different parts of the brain[42]. The connections between brain regions are summarized in the 3D color-coded reconstructions to the left. The nodes identified with vehicle treatment were reduced from 20 to 12 with multidose LD treatments while the connections were reduced from 22 to 14. This decrease in connectivity was

	Vehicle			LSD			
Brain area	Mean	SD		Mean	SD	P-Val	Ω Sq
Reticular thalamic n	1.51	0.06	<	1.59	0.09	0.006	0.291
Anterior cingulate n	1.94	0.10	>	1.82	0.06	0.006	0.289
Secondary motor ctx	2.11	0.13	>	1.98	0.09	0.010	0.247
Medial geniculate	1.39	0.05	<	1.46	0.09	0.022	0.185
CA3	1.80	0.32	<	1.92	0.12	0.022	0.185
4th cerebellar lobule	1.33	0.11	<	1.43	0.17	0.028	0.168
Central medial thalamic n	1.38	0.04	<	1.44	0.10	0.031	0.159
Lateral paragigantocellular n	2.41	0.66	>	1.89	0.30	0.033	0.157
CA1	1.70	0.18	<	1.76	0.08	0.043	0.136

Table 1. Apparent diffusion coefficient: vehicle vs single dose LSD.

	Vehicle			LSD			
Brain area	Mean	SD		Mean	SD	P-Val	Ω Sq
Vestibular n	1.53	0.09	<	1.73	0.11	0.000	0.650
Basal amygdaloid n	1.56	0.08	<	1.74	0.09	0.000	0.574
Dentate gyrus	1.56	0.06	<	1.70	0.10	0.000	0.520
Central medial thalamic n	1.38	0.04	<	1.51	0.11	0.000	0.520
Periaqueductal gray	1.55	0.07	<	1.72	0.14	0.001	0.509
Medial geniculate	1.39	0.05	<	1.53	0.13	0.001	0.499
Parafascicular thalamic n	1.39	0.05	<	1.54	0.11	0.001	0.480
Parabrachial n	1.41	0.05	<	1.55	0.14	0.001	0.469
Globus pallidus	1.39	0.05	<	1.52	0.10	0.001	0.450
Entorhinal ctx	1.53	0.08	<	1.71	0.12	0.001	0.449
Posterior thalamic n	1.36	0.05	<	1.49	0.12	0.001	0.440
Lateral posterior thalamic n	1.50	0.05	<	1.63	0.10	0.001	0.440
Reticular thalamic n	1.51	0.06	<	1.64	0.12	0.001	0.432
Zona incerta	1.48	0.05	<	1.61	0.13	0.001	0.423
Subiculum	1.56	0.08	<	1.72	0.12	0.001	0.422
Caudate putamen	1.46	0.09	<	1.62	0.10	0.002	0.403
Crus of ansiform lobule	1.28	0.10	<	1.44	0.15	0.002	0.395
Pedunculopontine tegmental n	1.46	0.09	<	1.63	0.12	0.002	0.393
External capsule	1.64	0.14	<	1.80	0.10	0.002	0.384
Mesencephalic reticular formation	1.43	0.05	<	1.56	0.13	0.003	0.369
5th cerebellar lobule	1.25	0.08	<	1.41	0.15	0.003	0.368
Locus coeruleus	1.73	0.24	<	2.14	0.30	0.003	0.367
Internal capsule	1.50	0.11	<	1.65	0.08	0.003	0.350
Corpus callosum	1.80	0.12	<	1.99	0.15	0.003	0.350
Ventral thalamic n	1.41	0.05	<	1.53	0.12	0.004	0.344
Solitary tract n	1.41	0.08	<	1.57	0.15	0.004	0.343
Anterior hypothalamic n	1.81	0.11	<	1.97	0.14	0.004	0.342
Lateral caudal hypothalamic n	1.61	0.09	<	1.75	0.12	0.004	0.341
Cerebellar nuclear n	1.39	0.05	<	1.53	0.17	0.005	0.318
Central amygdaloid n	1.57	0.11	<	1.81	0.19	0.005	0.317
Cerebral peduncle	1.48	0.07	<	1.61	0.14	0.005	0.317
Inferior colliculus	1.52	0.09	<	1.66	0.13	0.005	0.317
Bed nucleus stria terminalis	1.57	0.10	<	1.76	0.14	0.005	0.317
Cuneate n	1.64	0.17	<	1.89	0.19	0.005	0.316
Lateral preoptic n	1.48	0.09	<	1.62	0.11	0.006	0.309
Paramedian lobule	1.33	0.18	<	1.60	0.24	0.006	0.309
Anterior pretectal thalamic n	1.66	0.09	<	1.81	0.14	0.006	0.302
Auditory ctx	1.46	0.13	<	1.62	0.13	0.006	0.301
Lateral rostral hypothalamic n	1.54	0.09	<	1.66	0.11	0.007	0.293
6th cerebellar lobule	1.28	0.12	<	1.47	0.15	0.007	0.293
Dorsal hippocampal commissure	1.51	0.11	<	1.67	0.15	0.007	0.293
CA1	1.70	0.18	<	1.87	0.16	0.007	0.293
Dorsal raphe	1.51	0.08	<	1.65	0.13	0.008	0.278
Accumbens core	1.37	0.06	<	1.47	0.10	0.009	0.271
Stria terminalis	1.83	0.33	<	2.11	0.34	0.011	0.249
Medial preoptic n	1.78	0.15	<	1.96	0.13	0.012	0.248
Medial amygdaloid n	1.73	0.12	<	1.87	0.13	0.014	0.234
7th cerebellar lobule	1.34	0.27	<	1.56	0.23	0.015	0.226
Accumbens shell	1.37	0.05	<	1.46	0.11	0.016	0.221
Anterior commissure	1.46	0.09	<	1.58	0.13	0.016	0.220
Secondary somatosensory ctx	1.46	0.07	<	1.58	0.13	0.019	0.207
Parvicellular reticular n	1.57	0.14	<	1.74	0.19	0.019	0.206
8th cerebellar lobule	1.28	0.20	<	1.44	0.20	0.021	0.199
Lateral amygdaloid n	1.62	0.18	<	1.97	0.42	0.023	0.193
2nd cerebellar lobule	1.50	0.12	<	1.64	0.17	0.027	0.180
Continued							

Brain area	Vehicle			LSD			
	Mean	SD		Mean	SD	P-Val	Ω Sq
Caudal piriform ctx	1.62	0.10	<	1.74	0.15	0.027	0.180
Medial dorsal thalamic n	1.54	0.12	<	1.68	0.16	0.027	0.180
Lateral dorsal thalamic n	1.61	0.24	<	1.68	0.14	0.029	0.174
Lateral septal n	1.90	0.32	<	2.10	0.19	0.029	0.173
Lateral geniculate	1.49	0.10	<	1.58	0.10	0.031	0.168
Forceps minor corpus callosum	1.51	0.09	<	1.61	0.14	0.031	0.168
Superior colliculus	1.59	0.08	<	1.70	0.13	0.031	0.167
Diagonal band of Broca	1.51	0.09	<	1.61	0.13	0.033	0.163
Temporal ctx	1.41	0.13	<	1.56	0.18	0.033	0.162
Reuniens thalamic n	1.45	0.09	<	1.57	0.14	0.034	0.161
Substantia nigra	1.63	0.13	<	1.78	0.17	0.034	0.161
Extended amygdala	1.46	0.07	<	1.56	0.12	0.036	0.156
Medial lemniscus	1.68	0.12	<	1.82	0.14	0.036	0.155
Flocculus cerebellum	1.46	0.14	<	1.61	0.22	0.038	0.151
Infralimbic ctx	1.49	0.10	<	1.63	0.16	0.039	0.150
4th cerebellar lobule	1.33	0.11	<	1.42	0.16	0.045	0.138
Primary somatosensory ctx	1.77	0.10	<	1.86	0.13	0.049	0.133
Principal sensory n. trigeminal	1.64	0.12	<	1.79	0.17	0.049	0.132
CA3	1.80	0.32	<	1.96	0.26	0.049	0.132

Table 2. Apparent diffusion coefficient: vehicle vs multiple dose LSD.

directed to the basal ganglia, brainstem/cerebellar areas with LSD treatment in adolescence but not sensory motor cortices or hippocampus.

Discussion

Neuroplasticity, the changes in neuronal structure and connectivity together with the parenchymal microarchitecture, occurs throughout the developmental lifespan and in response to environmental stressors. Psychiatric patients[16] and healthy subjects[43] given LSD report long lasting effects on mental health and well-being. Changes in brain neuroplasticity are thought to be responsible for these protracted effects on behavior[18]. Indeed, hallucinogens e.g. LSD psilocybin, and DMT, have the capability to induce changes in brain functional connectivity and gray matter microarchitecture[18]. Nichols and coworkers reported LSD enhances the expression of genes with neurotrophic activity in the prefrontal ctx of rats[44]. Adolescence is accepted to be a vulnerable period in brain development as connections in the prefrontal cortex undergo sprouting, pruning and reorganization for participation in executive control and impulse inhibition[45]. How does exposure to a drug like LSD with inherent neuroplastic activity alter the natural developmental organization and trajectory of the adolescent brain? We addressed this question by giving female and male mice an oral gavage of vehicle, single exposure to LSD, or multiple exposures of LSD over several days. Any long-lasting changes in neuroplasticity were evaluated several weeks later using multimodal MRI and behavioral assays. Our findings are discussed in the context of previous longitudinal studies in rodents and more importantly, humans.

Behavior

When compared across all three treatment groups, Open Field Test (OFT) revealed differences in time spent in the center zone for mice treated with a single dose of LSD versus vehicle or multidose LSD conditions. The amount of time spent in the center zone during OFT is known to assess differences in anxiety[46]. Based on our findings, a single-dose of LSD during late adolescence may have a long-term anxiolytic effect on mice. These findings warrant further investigation of LSD as a long-term treatment for anxiety in late adolescent humans (age 18–25). As observed in the OFT, total distance traveled was not significantly different across all experimental conditions.

Novel Object Preference (NOP) testing is used to investigate memory and learning in mice[47]. A prolonged period (greater than 8 h) between familiarization and testing have been extensively used to evaluate long-term memory in rodents[48–51]. All three experimental groups performed better than chance spending significantly more time investigating the novel object. However, the more subtle behavioral measures of latency to approach the novel object and duration of time spent with the familiar object during a single encounter or bout were significantly different between groups and only realized in mice given multiple doses of LSD in adolescence. We have no explanation for these behaviors in the context of cognition or emotion. Ornelas and coworkers studied the cognitive effects of a single dose of LSD (130 µg/kg) given to young, adult, or old male rats evaluated for NOP[52]. To avoid psychotomimetic effects, rats were evaluated several days after LSD exposure. All age groups showed a significant preference for the novel object as compared to saline treated controls. To the best of our knowledge there have been no neuroplasticity studies in rodents looking at the long-term effects of LSD on

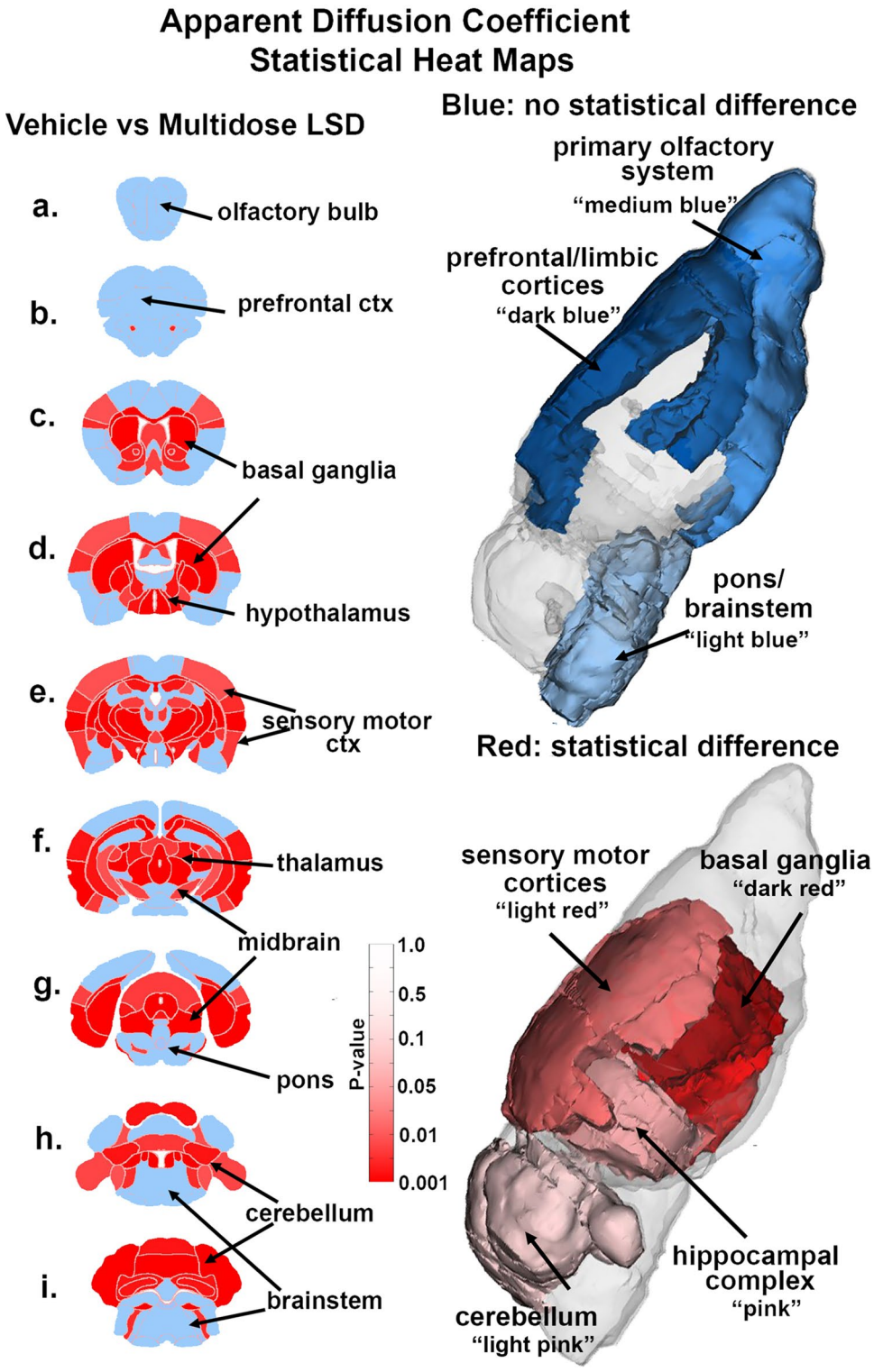

Figure 2. Apparent diffusion coefficient. Shown are 2D images of statistical heat maps showing the location of brain regions that were significantly different in ADC values between multidose LSD and vehicle. Areas in red denote a significant increase in ADC values over vehicle for LSD treatment. The blue denotes areas that were unaffected by LSD treatment emphasizing the olfactory bulb, prefrontal cortex and brainstem. The 3D color coded reconstructions to the right summarize these regional difference in measures of ADC.

Brain area	Vehicle			LSD			
	Ave	SD		Ave	SD	P-Val	Ω Sq
Lateral caudal hypothalamic n	0.48	0.03	>	0.43	0.03	0.002	0.390
Reticular thalamic n	0.43	0.02	>	0.41	0.03	0.022	0.188
Temporal ctx	0.30	0.03	<	0.34	0.06	0.026	0.175
Secondary motor ctx	0.21	0.02	<	0.24	0.06	0.035	0.152
Globus pallidus	0.33	0.03	>	0.31	0.03	0.035	0.151
Lateral rostral hypothalamic n	0.42	0.03	>	0.39	0.03	0.035	0.150
Interpeduncular n	0.32	0.04	>	0.29	0.03	0.039	0.143
7th cerebellar lobule	0.32	0.02	<	0.36	0.05	0.042	0.138
Stria terminalis	0.45	0.08	<	0.51	0.07	0.046	0.131
Habenular n	0.37	0.05	<	0.41	0.04	0.046	0.131
Tenia tecta ctx	0.30	0.04	>	0.27	0.02	0.048	0.128

Table 3. Fractional anisotropy: vehicle vs single dose LSD.

Brain area	Vehicle			LSD			
	Ave	SD		Ave	SD	P-Val	Ω Sq
Medial mammillary n	0.32	0.02	>	0.28	0.03	0.001	0.439
Lateral caudal hypothalamic n	0.48	0.03	>	0.43	0.03	0.004	0.338
Vestibular n	0.33	0.02	>	0.30	0.03	0.005	0.315
CA1	0.30	0.03	>	0.26	0.02	0.006	0.303
Cerebellar nuclear n	0.36	0.04	>	0.32	0.02	0.009	0.272
Pedunculopontine tegmental n	0.33	0.03	>	0.29	0.03	0.011	0.250
Lateral posterior thalamic n	0.32	0.05	>	0.28	0.04	0.013	0.235
10th cerebellar lobule	0.28	0.02	>	0.26	0.04	0.019	0.209
Medial lemniscus	0.33	0.02	>	0.28	0.06	0.023	0.191
Principal sensory n. trigeminal	0.44	0.04	>	0.40	0.02	0.033	0.163
Solitary tract n	0.37	0.04	>	0.33	0.05	0.035	0.157
Basal amygdaloid n	0.34	0.03	>	0.33	0.02	0.037	0.153
Parabrachial n	0.37	0.04	>	0.33	0.04	0.037	0.153
Locus coeruleus	0.32	0.04	>	0.28	0.05	0.039	0.150
Pontine reticular nucleus oral	0.32	0.02	>	0.29	0.03	0.040	0.148
Reticulotegmental nucleus	0.29	0.03	>	0.26	0.03	0.043	0.141
Posterior thalamic n	0.31	0.03	>	0.27	0.04	0.048	0.134

Table 4. Fractional anisotropy: vehicle vs multidose dose LSD.

cognitive behavior beyond several days. This is also true for humans. Our study imaged mice between six to eight weeks post LSD treatment. This period of time between treatment and testing in mice would be approximately 5 -7 years in a human life[53].

Brain volume

Again, to the best of our knowledge, this is the first study to look at LSD-induced developmental changes in brain volume using voxel-based morphometry in animals or humans. Using a 3D mouse MRI atlas with 139 segmented brain areas and computational analysis we were unable to find significantly relevant changes when taking into consideration false discovery rates and effect sizes. The study compared vehicle controls to a single dose of LSD (3.3 µg) given orally once or multiple times over several days. Would a higher dose of LSD have altered the brain development as reflected by changes in the volume of specific brain areas?

Diffusion weighted imaging

Using DWI to study the developmental effects of LSD has no precedent in the animal or human literature. Indices of anisotropy like ADC and FA provide numerical measures of water movement and give insight into the micro-architecture of tissue. An increase in ADC values and decrease in FA values indicate less restriction on water movement and suggest a less dense gray matter microarchitecture. Here we show that exposure to LSD during adolescence leads to a significant increase in ADC values across much of the brain with a smaller number of brain areas showing a decrease in FA values. DWI is routinely used to assess white matter integrity after a head injury[54]. Changes in ADC and FA values have been used to track subtle alterations in gray matter microarchitecture after a head injury, helping to pinpoint areas of neuroinflammation in the brain[55,56]. Correlations between

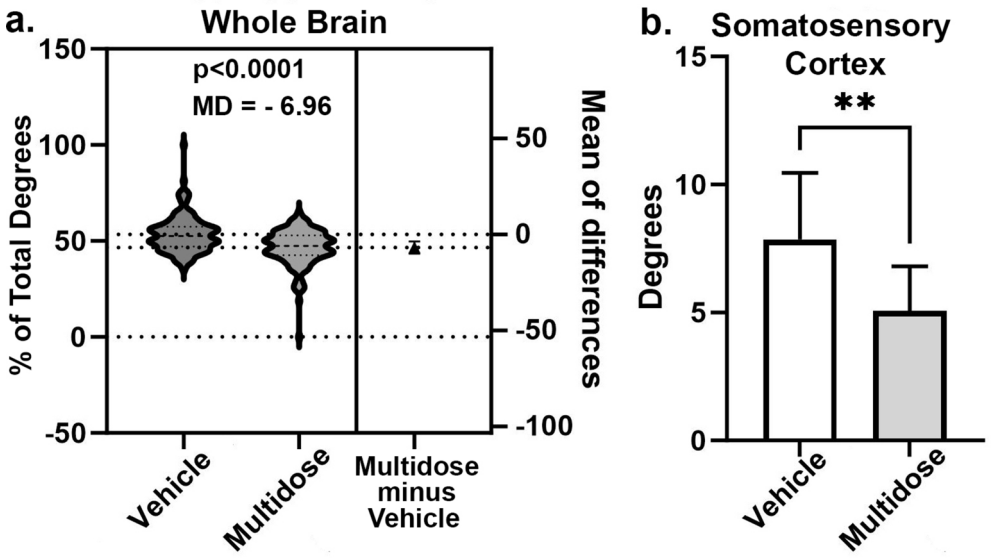

Figure 3. Global functional connectivity. (**a**) The percentage change in degrees (connections) for all 139 brain areas between multidose LSD and vehicle controls are shown as violin plots for vehicle and multidose LSD treatments. The multidose treatment showed mean difference (MD) of 6.96 percent less than vehicle and had significantly fewer connections (two-tailed, paired t-test, $p < 0.0001$). When the 139 brain areas were organized into 12 brain regions (Supplementary Data Fig S1), there were no significant differences in degrees between vehicle and multidose groups with the exception of the somatosensory cortex (**b**). (**b**) The mean ± SD for the number of degrees in the somatosensory cortex for veh as compared to the multidose group. (**$p < 0.01$).

measures of FA and ADC have also been employed to describe the organization of brain tumors[57]. In a recent study, Coleman et al. showed a unique correlation between ADC and FA values in the forebrain and hindbrain of female, but not male mice, exposed to chronic inhaled vaporized cannabis throughout adolescence[32]. In this cannabis study the elevated FA and decreased ADC values suggested a more organized prefrontal cortex in female mice exposed to cannabis high in THC during adolescence. It should be noted, in our study here, there were no significant differences in measures of anisotropy between male and female mice given multidose LSD in adolescence. The absence in any sex difference is consistent with the human literature[58]. Indeed, there are no sex differences in the pharmacokinetics of oral LSD in healthy men and women[59].

The simple explanation for the DWI results is the homeostatic regulation of fluid balance between the intracellular and extracellular compartments. In this case the increased ADC would suggest an increase in the extracellular volume. A more complex explanation would be a decrease in the number of glial and/or neurons, or a reduction in dendritic branching, dendritic spines, perineuronal nets, capillary density, and extracellular matrix. However, there is a prevailing hypothesis that LSD and other hallucinogens that target the 5-HT2a receptor enhance long lasting neuroplastic changes in the brain[18,60]. There is compelling evidence in support of this notion from molecular studies on the activation of genes associated with neurogenesis[44,61,62]. The effects of repeated exposure to low dose LSD in adolescence on the molecular biology of neurogenesis has never been studied.

Resting state functional connectivity

From the general pattern of brain functional connectivity there was little evidence of consequential changes across experimental groups for any particular brain region. When all 139 brain areas were paired between vehicle and multidose and normalized to percentage change there was a whole brain decrease in the number of connections by little less than seven percent for multidose LSD. Yet out of 16 brain regions e.g. hypothalamus, PFC, midbrain, thalamus, cerebellum, etc., only the areas comprising the somatosensory ctx were significantly less than vehicle. Thus, there is a subtle but significant decrease in global connectivity. Are fewer connections better? The corpus callosum together with the forceps minor and the external capsule, white matter tracts associated with the corpus callosum, showed the greatest decrease in the number of degrees. The forceps minor extends from the anterior part of the corpus callosum and projects into the frontal lobes and functions to facilitate communication between the left and right frontal lobes. The external capsule has white matter fibers that originate and project to the corpus callous and conveys information to different parts of the cerebral cortex. Given this core of white fiber tracts originating in the corpus callosum we analyzed them together as a single node. With vehicle treatment in adolescence (see Fig. 4) this white matter node showed extensive connections to multiple areas some like the brainstem and cerebellum, with long pathways. Local multidose LSD network analysis examining the corpus callosum in adolescence resulted in a pattern of connectivity that favored the same eight cortical brain areas and hippocampal areas while eliminating areas further in distance. This anatomical topography of local clustering and short path lengths is thought to be bioenergetically more economical than multiple nodes spread out over larger areas[63]. There are no long-term (years) studies in humans looking at changes in functional connectivity to

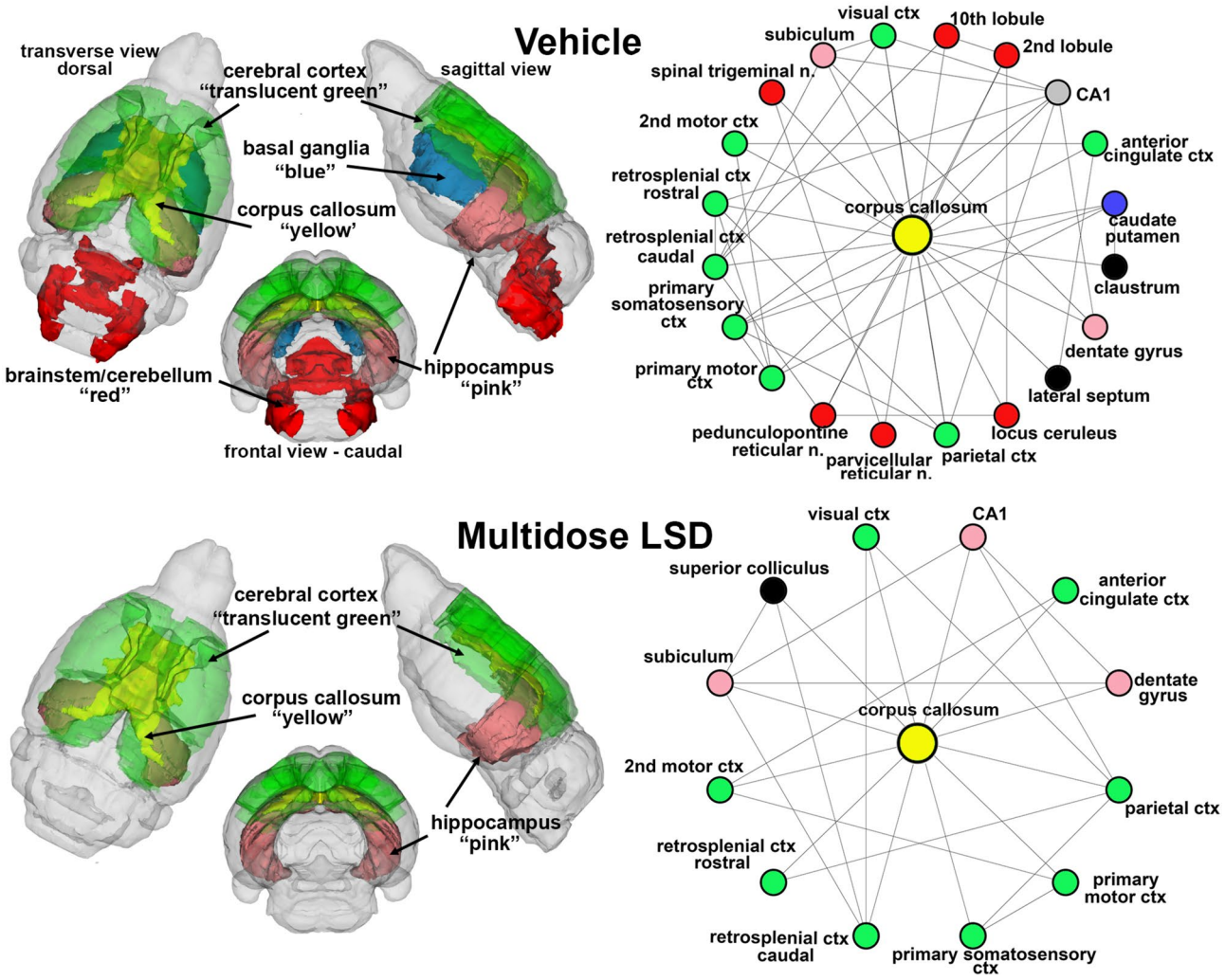

Figure 4. White matter connectivity. The radial connectivity diagrams show the connections (lines) to different nodes (colored circles) from the corpus callosum (yellow) comparing vehicle to multidose LSD. Circles in green highlight brain areas comprising the cerebral cortex. Circles in red are brain areas located in the brainstem and cerebellum while those in pink are hippocampal brain areas. Area in black are not associated with these other brain regions. The color-coded 3D representation shows the location of these brain areas providing a visual summary of their difference between experimental groups and location.

earlier LSD exposure. However, there have been several studies looking at the acute effects of LSD on connectivity. Healthy volunteers injected IV with 75 µg of LSD show an increase in global connectivity between networks, but a decrease in connectivity within networks[8,64]. These results were corroborated in healthy volunteers given an oral dose of 100 µg of LSD[9,10].

Data interpretation and limitations

Our findings are predicated on a single dose of LSD of 3.3 µg/100 µl give to all animals across body weights ranging from 20 to 24 g. This was judged to be a moderate dose based on the literature[27–30]. At the time of treatment there was no effort to collect blood samples because we did not want to add any more stress to that already caused by the oral gavages. Would higher or lower doses of LSD given more often have a greater impact on development?

As a developmental study it would have been highly informative if we had molecular information comparing the genes and proteins associated with neurogenesis between experimental groups. This would also be true of histological measures for numerous markers of neuroplasticity that could have helped interpret the DWI data. These were meant to be end-of life studies, using non-invasive MRI to follow brain structure and function with aging. In addition, efforts to image mice while fully awake in response to fear and reward stimuli were unsuccessful and a majority of the multidose animals died or were lost with aging, precluding sample collection. With respect to development, are the results unique to adolescence or would we have gotten similar or different data in middle aged adults or old mice? When adolescent, adult, and old mice are chronically exposed to the vapor of the same cannabis plant yielding similar blood levels of THC, each developmental period presents with different structural and functional data gleaned from multimodal MRI[32,34,35].

Our assessment of cognitive and motor behavior was limited to NOP and OFT, respectively. It is very possible we could have parsed out more differences between groups if we used a battery of behavior test or altered the conditions of our assays. For example, in the NOP the interval between testing is critical as some mice cannot discriminate objects after 8 h intervals as used in this study[65], while other studies have used interval periods up to 24 h to investigate long-term memory consolidation in mice[48–50,66,67]. While a single dose of LSD gave some evidence of reduced anxiety, our study would have benefited from a battery of behavioral tests to assess emotion and motivation. Indeed, the absence of any differences in measures of behavior should not be taken as evidence of no behavioral changes but must take into consideration the limitations set by experimental conditions and techniques. Using these limited experimental assays does not disqualify LSD from having long-term effects on behavior.

Conclusion

This is the first study to use non-invasive MRI to evaluate the developmental effects of LSD given during peri-adolescence. The effects of a single exposure were inconsequential, but exposure to multiple doses over several days had long lasting effects on gray matter microarchitecture and functional connectivity later in life. These changes were not reflected in any gross dysfunctional changes in cognitive or motor behavior. However, are there more subtle deficits or benefits in cognitive, emotional and motor behaviors to periadolescent exposure to LSD? This remains to be explored. There are ongoing studies using hallucinogens to treat psychiatric disorders[68]. It is critical that we fill in these knowledge gaps to support the validity and safety of clinical practice.

Data availability

Availability of data and materials: all voxel based morphometry and diffusion weighted imaging data generated or analyzed during this study are included in this published article [and its supplementary information files]. The functional connectivity data are available through Dryad https://doi.org/10.5061/dryad.9kd51c5s9.

Received: 22 February 2024; Accepted: 7 August 2024
Published online: 11 August 2024

References

1. Nichols, D. E. & Walter, H. The history of psychedelics in psychiatry. *Pharmacopsychiatry* **54**, 151–166 (2021).
2. Carhart-Harris, R. L. & Goodwin, G. M. The therapeutic potential of psychedelic drugs: Past, present, and future. *Neuropsychopharmacology* **42**, 2105–2113 (2017).
3. Ross, S. *et al.* Psychedelic-assisted psychotherapy to treat psychiatric and existential distress in life-threatening medical illnesses and palliative care. *Neuropharmacology* **216**, 109174 (2022).
4. Ferris, C. F., Kulkarni, P., Yee, J. R., Nedelman, M. & de Jong, I. E. M. The serotonin receptor 6 antagonist idalopirdine and acetylcholinesterase inhibitor donepezil have synergistic effects on brain activity—A functional MRI study in the awake rat. *Front. Pharmacol.* **8**, 279 (2017).
5. Iriah, S. C. *et al.* Oxycodone exposure: A magnetic resonance imaging study in response to acute and chronic oxycodone treatment in rats. *Neuroscience* **398**, 88–101 (2019).
6. Kawazoe, K. *et al.* Dose-dependent effects of esketamine on brain activity in awake mice: A BOLD phMRI study. *Pharmacol. Res. Perspect.* **10**, e01035 (2022).
7. Sadaka, A. H. *et al.* Cannabidiol has a unique effect on global brain activity: A pharmacological, functional MRI study in awake mice. *J. Transl. Med.* **19**, 220 (2021).
8. Carhart-Harris, R. L. *et al.* Neural correlates of the LSD experience revealed by multimodal neuroimaging. *Proc. Natl. Acad. Sci. USA* **113**, 4853–4858 (2016).
9. Muller, F. *et al.* Increased thalamic resting-state connectivity as a core driver of LSD-induced hallucinations. *Acta Psychiatr. Scand.* **136**, 648–657 (2017).
10. Preller, K. H. *et al.* Changes in global and thalamic brain connectivity in LSD-induced altered states of consciousness are attributable to the 5-HT2A receptor. *Elife* **7**, 6 (2018).
11. Muller, F., Dolder, P. C., Schmidt, A., Liechti, M. E. & Borgwardt, S. Altered network hub connectivity after acute LSD administration. *Neuroimage Clin.* **18**, 694–701 (2018).
12. Preller, K. H. *et al.* Effective connectivity changes in LSD-induced altered states of consciousness in humans. *Proc. Natl. Acad. Sci. USA* **116**, 2743–2748 (2019).
13. Preller, K. H. *et al.* Role of the 5-HT(2A) receptor in self- and other-initiated social interaction in lysergic acid diethylamide-induced states: A pharmacological fMRI study. *J. Neurosci.* **38**, 3603–3611 (2018).
14. Carhart-Harris, R. L. *et al.* Psilocybin with psychological support for treatment-resistant depression: Six-month follow-up. *Psychopharmacology (Berl)* **235**, 399–408 (2018).
15. Ross, S. *et al.* Rapid and sustained symptom reduction following psilocybin treatment for anxiety and depression in patients with life-threatening cancer: A randomized controlled trial. *J. Psychopharmacol.* **30**, 1165–1180 (2016).
16. Gasser, P., Kirchner, K. & Passie, T. LSD-assisted psychotherapy for anxiety associated with a life-threatening disease: A qualitative study of acute and sustained subjective effects. *J. Psychopharmacol.* **29**, 57–68 (2015).
17. Johnson, M. W., Garcia-Romeu, A. & Griffiths, R. R. Long-term follow-up of psilocybin-facilitated smoking cessation. *Am. J. Drug Alcohol Abuse* **43**, 55–60 (2017).
18. Calder, A. E. & Hasler, G. Towards an understanding of psychedelic-induced neuroplasticity. *Neuropsychopharmacology* **48**, 104–112 (2023).
19. Ly, C. *et al.* Psychedelics promote structural and functional neural plasticity. *Cell Rep.* **23**, 3170–3182 (2018).
20. Bates, M. L. S. & Trujillo, K. A. Use and abuse of dissociative and psychedelic drugs in adolescence. *Pharmacol. Biochem. Behav.* **203**, 173129 (2021).
21. Blakemore, S.-J. & Choudhury, S. Development of the adolescent brain: Implications for executive function and social cognition. *J. Child Psychol. Psychiatry* **47**, 296–312 (2006).
22. Sowell, E. R., Thompson, P. M., Tessner, K. D. & Toga, A. W. Mapping continued brain growth and gray matter density reduction in dorsal frontal cortex: Inverse relationships during postadolescent brain maturation. *J. Neurosci.* **21**, 8819–8829 (2001).
23. Petanjek, Z. *et al.* Extraordinary neoteny of synaptic spines in the human prefrontal cortex. *Proc. Natl. Acad. Sci. USA* **108**, 13281–13286 (2011).

24. Livne, O., Shmulewitz, D., Walsh, C. & Hasin, D. S. Adolescent and adult time trends in US hallucinogen use, 2002–19: Any use, and use of ecstasy, LSD and PCP. *Addiction* **117**, 3099–3109 (2022).
25. Romeo, R. D., Patel, R., Pham, L. & So, V. M. Adolescence and the ontogeny of the hormonal stress response in male and female rats and mice. *Neurosci. Biobehav. Rev.* **70**, 206–216 (2016).
26. Kilkenny, C., Browne, W. J., Cuthill, I. C., Emerson, M. & Altman, D. G. Improving bioscience research reporting: The ARRIVE guidelines for reporting animal research. *PLoS Biol.* **8**, e1000412 (2010).
27. De Gregorio, D. *et al.* The hallucinogen D-lysergic diethylamide (LSD) decreases dopamine firing activity through 5-HT(1A), D(2) and TAAR(1) receptors. *Pharmacol. Res.* **113**, 81–91 (2016).
28. Inserra, A. *et al.* Lysergic acid diethylamide differentially modulates the reticular thalamus, mediodorsal thalamus, and infralimbic prefrontal cortex: An in vivo electrophysiology study in male mice. *J. Psychopharmacol.* **35**, 469–482 (2021).
29. Pieri, L., Pieri, M. & Haefely, W. LSD as an agonist of dopamine receptors in the striatum. *Nature* **252**, 586–588 (1974).
30. De Gregorio, D. *et al.* Lysergic acid diethylamide (LSD) promotes social behavior through mTORC1 in the excitatory neurotransmission. *Proc. Natl. Acad. Sci. USA* **118**, 34 (2021).
31. Ferris, C. F. *et al.* Studies on the Q175 knock-in model of Huntington's disease using functional imaging in awake mice: Evidence of olfactory dysfunction. *Front. Neurol.* **5**, 94 (2014).
32. Coleman, J. R. *et al.* Changes in brain structure and function following chronic exposure to inhaled vaporised cannabis during periadolescence in female and male mice: A multimodal MRI study. *Addict. Biol.* **27**, e13169 (2022).
33. Otto, L. D. *et al.* Paclitaxel chemotherapy elicits widespread brain anisotropy changes in a comprehensive mouse model of breast cancer survivorship: Evidence from in vivo diffusion weighted imaging. *Front. Oncol.* **12**, 798704 (2022).
34. Taylor, A. *et al.* Chronic exposure to inhaled vaporized cannabis high in Delta9-THC alters brain structure in adult female mice. *Front. Neurosci.* **17**, 1139309 (2023).
35. Sadaka, A. H. *et al.* Effects of inhaled cannabis high in Delta9-THC or CBD on the aging brain: A translational MRI and behavioral study. *Front. Aging Neurosci.* **15**, 1055433 (2023).
36. Ortiz, R. J. *et al.* Functional connectivity differences between two culturally distinct prairie vole populations: Insights into the prosocial network. *Biol. Psychiatry Cogn. Neurosci. Neuroimaging* **7**, 576–587 (2022).
37. Gorges, M. *et al.* Functional connectivity mapping in the animal model: Principles and applications of resting-state fMRI. *Front. Neurol.* **8**, 200 (2017).
38. Liang, Z., King, J. & Zhang, N. Intrinsic organization of the anesthetized brain. *J. Neurosci.* **32**, 10183–10191 (2012).
39. Poser, B. A. & Norris, D. G. Investigating the benefits of multi-echo EPI for fMRI at 7 T. *Neuroimage* **45**, 1162–1172 (2009).
40. Iriah, S. C. *et al.* The utility of maraviroc, an antiretroviral agent used to treat HIV, as treatment for opioid abuse? Data from MRI and behavioural testing in rats. *J. Psychiatry Neurosci.* **46**, E548–E558 (2021).
41. Bastian, M., Heymann, S. & Jacomy, M. Gephi: An open source software for exploring and manipulating networks. In *International AAAI Conference on Weblogs and Social Media* (2009).
42. Smith, J. B., Lee, A. K. & Jackson, J. The claustrum. *Curr. Biol.* **30**, R1401–R1406 (2020).
43. Schmid, Y. *et al.* Acute effects of lysergic acid diethylamide in healthy subjects. *Biol. Psychiatry* **78**, 544–553 (2015).
44. Nichols, C. D., Garcia, E. E. & Sanders-Bush, E. Dynamic changes in prefrontal cortex gene expression following lysergic acid diethylamide administration. *Brain Res. Mol. Brain Res.* **111**, 182–188 (2003).
45. Sowell, E. R., Trauner, D. A., Gamst, A. & Jernigan, T. L. Development of cortical and subcortical brain structures in childhood and adolescence: A structural MRI study. *Dev. Med. Child Neurol.* **44**, 4–16 (2002).
46. Kraeuter, A. K., Guest, P. C. & Sarnyai, Z. The open field test for measuring locomotor activity and anxiety-like behavior. *Methods Mol. Biol.* **1916**, 99–103 (2019).
47. Lueptow, L.M. Novel object recognition test for the investigation of learning and memory in mice**.** *J. Vis. Exp.* (2017).
48. Botton, P. H. *et al.* Caffeine prevents disruption of memory consolidation in the inhibitory avoidance and novel object recognition tasks by scopolamine in adult mice. *Behav. Brain Res.* **214**, 254–259 (2010).
49. Moore, S. J., Deshpande, K., Stinnett, G. S., Seasholtz, A. F. & Murphy, G. G. Conversion of short-term to long-term memory in the novel object recognition paradigm. *Neurobiol. Learn Mem.* **105**, 174–185 (2013).
50. Hale, G. & Good, M. Impaired visuospatial recognition memory but normal object novelty detection and relative familiarity judgments in adult mice expressing the APPswe Alzheimer's disease mutation. *Behav. Neurosci.* **119**, 884–891 (2005).
51. Morrison, T. R. *et al.* Treating head injury using a novel vasopressin 1a receptor antagonist. *Neurosci. Lett.* **714**, 134565 (2020).
52. Ornelas, I. M. *et al.* Nootropic effects of LSD: Behavioral, molecular and computational evidence. *Exp. Neurol.* **356**, 114148 (2022).
53. Dutta, S. & Sengupta, P. Men and mice: Relating their ages. *Life Sci.* **152**, 244–248 (2016).
54. Messe, A. *et al.* Diffusion tensor imaging and white matter lesions at the subacute stage in mild traumatic brain injury with persistent neurobehavioral impairment. *Hum. Brain Mapp.* **32**, 999–1011 (2011).
55. Kulkarni, P. *et al.* Evidence of early vasogenic edema following minor head impact that can be reduced with a vasopressin V1a receptor antagonist. *Brain Res. Bull.* **165**, 218–227 (2020).
56. Kulkarni, P. *et al.* Use of anisotropy, 3D segmented atlas, and computational analysis to identify gray matter subcortical lesions common to concussive injury from different sites on the cortex. *PLoS One* **10**, e0125748 (2015).
57. De Belder, F. E. *et al.* Diffusion tensor imaging provides an insight into the microstructure of meningiomas, high-grade gliomas, and peritumoral edema. *J. Comput. Assist. Tomogr.* **36**, 577–582 (2012).
58. Holze, F. *et al.* Acute dose-dependent effects of lysergic acid diethylamide in a double-blind placebo-controlled study in healthy subjects. *Neuropsychopharmacology* **46**, 537–544 (2021).
59. Dolder, P. C., Schmid, Y., Haschke, M., Rentsch, K. M. & Liechti, M. E. Pharmacokinetics and concentration–effect relationship of oral LSD in humans. *Int. J. Neuropsychopharmacol.* **19**, 6 (2015).
60. Olson, D. E. Psychoplastogens: A promising class of plasticity-promoting neurotherapeutics. *J. Exp. Neurosci.* **12**, 1179069518800508 (2018).
61. Gonzalez-Maeso, J. *et al.* Transcriptome fingerprints distinguish hallucinogenic and nonhallucinogenic 5-hydroxytryptamine 2A receptor agonist effects in mouse somatosensory cortex. *J. Neurosci.* **23**, 8836–8843 (2003).
62. Vaidya, V. A., Marek, G. J., Aghajanian, G. K. & Duman, R. S. 5-HT2A receptor-mediated regulation of brain-derived neurotrophic factor mRNA in the hippocampus and the neocortex. *J. Neurosci.* **17**, 2785–2795 (1997).
63. Bassett, D. S. & Bullmore, E. T. Small-world brain networks revisited. *Neuroscientist* **23**, 499–516 (2017).
64. Tagliazucchi, E. *et al.* Increased global functional connectivity correlates with LSD-induced ego dissolution. *Curr. Biol.* **26**, 1043–1050 (2016).
65. Akkerman, S., Blokland, A. & Prickaerts, J. Mind the gap: Delayed manifestation of long-term object memory improvement by phosphodiesterase inhibitors. *Neurobiol. Learn. Mem.* **109**, 139–143 (2014).
66. Antunes, M. & Biala, G. The novel object recognition memory: Neurobiology, test procedure, and its modifications. *Cogn. Process* **13**, 93–110 (2012).
67. Leger, M. *et al.* Object recognition test in mice. *Nat. Protoc.* **8**, 2531–2537 (2013).
68. de Wit, H., Molla, H. M., Bershad, A., Bremmer, M. & Lee, R. Repeated low doses of LSD in healthy adults: A placebo-controlled, dose-response study. *Addict. Biol.* **27**, e13143 (2022).

Acknowledgements
We thank the National Institute on Drug Abuse and Research Triangle Institute for providing the LSD used in these studies.

Author contributions
L.H.-B., Z.S., D.A., R.J. O., and A. C. performed the work and data analysis. L.H.-B., C.F.F. and P.P.K. contributed to the concept, experimental design, drafting, manuscript preparation and interpretation. All authors reviewed the manuscript.

Funding
Supported by Ekam Imaging.

Competing interests
CFF and PPK have a partnership interest in Ekam Solutions a company that develops 3D MRI atlases and makes radiofrequency electronics and holders for awake animal imaging. All other authors declare no competing interests.

Additional information
Supplementary Information The online version contains supplementary material available at https://doi.org/10.1038/s41598-024-69597-9.

Correspondence and requests for materials should be addressed to C.F.F.